

## The new generation of SPAD—Single-Photon Avalanche Diodes arrays<sup>(\*)</sup>

S. TUDISCO<sup>(1)</sup>, S. PRIVITERA<sup>(2)</sup>, L. LANZANÒ<sup>(2)</sup>, F. MUSUMECI<sup>(2)</sup>, A. PLUCHINO<sup>(2)</sup>,  
A. SCORDINO<sup>(2)</sup>, L. COSENTINO<sup>(1)</sup>, P. FINOCCHIARO<sup>(1)</sup>, G. CONDORELLI<sup>(3)</sup>,  
M. MAZZILLO<sup>(3)</sup>, S. LOMBARDO<sup>(4)</sup> and E. SCIACCA<sup>(4)</sup>

<sup>(1)</sup> INFN - Laboratori Nazionali del Sud - Via S. Sofia 65, 95100 Catania, Italy

<sup>(2)</sup> DMFCI and Dipartimento di Fisica ed Astronomia, Università di Catania  
Viale A. Doria 6, 95100 Catania, Italy

<sup>(3)</sup> ST-Microelectronics - Stradale Primosole 50, 95100 Catania, Italy

<sup>(4)</sup> IMM-CNR - Stradale Primosole 50, 95100 Catania, Italy

(ricevuto il 3 Marzo 2008; pubblicato online il 29 Aprile 2008)

**Summary.** — In the last years the single-photon detection with silicon devices has become an important goal. Here we present the performance of a new generation of single-photon avalanche diodes manufactured by ST-Microelectronics. The  $5 \times 5$  array configuration has been also realized and the performances, in terms of cross-talk and common readout mode, have been investigated.

PACS 42.79.Pw – Imaging detectors and sensors.

PACS 85.60.Gz – Photodetectors (including infrared and CCD detectors).

PACS 85.60.Dw – Photodiodes; phototransistors; photoresistors.

### 1. – Introduction

Several groups have been investigating for long time the possibility to build a silicon-based device suitable for single-photon counting applications [1-7]. Such a detector can be implemented by means of a  $p$ - $n$  junction biased above the breakdown voltage, so that a single photo-generated carrier can trigger an avalanche process through the junction. Main features of a Single-Photon Avalanche Diode (SPAD) are a uniform breakdown through the active area and controlled noise levels. Moreover, present-day technology allows SPADs to be integrated together with their quenching mechanisms which restore detector initial conditions after each avalanche process.

So integration of multiple sensors on the same substrate can be carried out, with common readout, realizing what is called a Silicon Photo-Multiplier (SiPM) [8, 9].

---

<sup>(\*)</sup> Paper presented at the 1st Workshop on Photon Detection for High Energy Medical and Space Applications; Perugia, June 13-14, 2007.

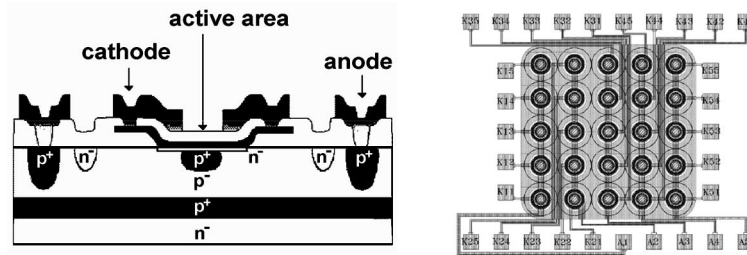


Fig. 1. – Left: vertical cross-section of the SPAD device. Right:  $5 \times 5$  array layout.

First, characteristics of the single SPAD sensors must be overviewed, since they affect performances of the integrated device. The cross-section structure of a SPAD device is depicted in fig. 1 along with the layout of a  $5 \times 5$  sensors array. SPAD sensors described here have been manufactured by ST-Microelectronics in Catania, through a process whose details can be found elsewhere [10-14]. Accurate processing steps allow to reach a good uniformity of the electric field over the whole active area, an important issue for the high SPAD quality since the quantum detection efficiency (QE) of the device must be independent of the absorption location.

In operating conditions, the supply voltage exceeds the breakdown value of an amount called Excess Bias Voltage (EBV) or overvoltage, which has fundamental influence on the detector performance. Since a higher electric field enhances the probability to trigger the avalanche, the Photon Detection Efficiency (PDE) increases with the overvoltage. At room temperature, for 20% of EBV, measured PDE is about: 50% at 550 nm, 10% at 850 nm and 3% at 1000 nm [15]. In order to operate properly a SPAD requires a suitable quenching circuit which stops the triggered avalanche process. In this case Passive-Quenching Circuit (PQC) was used so that the avalanche current is quenched itself by increasing a voltage drop on a high impedance load [16]. In appropriate conditions [17] the pulse waveform is directly determined by the diode current. So the fast rising time of the pulse, about few hundreds of picoseconds, is due to the avalanche formation, while the slower falling time is determined by the quenching mechanism. Active quenching electronics lead to the best timing resolution [18], on the other hand, PQC is simpler to integrate on board and relative performances are still quite good [17, 19]. In fact, resolution is about 160 ps (FWHM) in single-photon regime. A measure of the total number of elementary charges flowing during the avalanche allowed us to estimate a gain of the order of  $10^7$ .

An important parameter determining the actual quality of a SPAD is the level of noise. The detector noise is generally due to i) uncorrelated dark counts arising by the thermal carriers generation and ii) correlated pulses, due to trapping and delayed releasing of avalanche carriers from deep levels inside the junction.

Regarding the thermal noise, dark counts increase with both the temperature and the detector dimensions.

Typical values of dark counting rate at room temperature and 10–15% of EBV are 400 cps and 2000 cps for active areas  $20 \mu\text{m}$  and  $40 \mu\text{m}$  wide, respectively.

The dependence on the excess voltage and temperature is reported in the left part of fig. 2. Correlated noise arises because, during the avalanche process, some carriers may be captured by deep levels of the depletion region and subsequently released with a statistically fluctuating delay, whose mean value depends on the actually involved

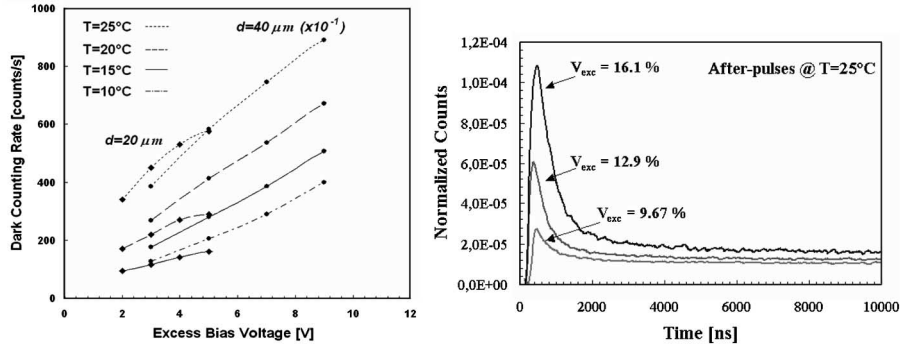


Fig. 2. – Left: dark counting rate as a function of the excess bias voltage, for passively quenched SPAD of active area with diameters  $d = 20 \mu\text{m}$  ( $\blacklozenge$ ) or  $d = 40 \mu\text{m}$  ( $\bullet$ ), at different temperatures:  $T = 25^\circ$  (dotted),  $T = 20^\circ$  (dashed),  $T = 15^\circ$  (solid),  $T = 10^\circ$  (dash-dotted). To plot both the sets of data, counts arising from the bigger device were reduced by a factor 10. Right: timing distribution of the correlated events, for the three particular EBV values and at room temperature. Counts were normalized to the total number of primary events.

levels [19]. Released carriers may then trigger a new avalanche and generate the so-called afterpulses. The number of carriers trapped during an avalanche increases with the total number of carriers crossing the junction, so more afterpulses are expected with increasing quenching delay and higher current intensities. For our devices, provided with PQC, the avalanche current is proportional to the EBV value, which is generally fixed in order to obtain the best detection efficiency and/or timing performance [15, 17]. Afterpulsing effects can be controlled through processing technologies able to reduce both the number of generation and recombination centres and minimize the concentration of trapping levels.

A detailed evaluation of the afterpulses contribution on passively quenched  $20 \mu\text{m}$  devices has been performed. The time distributions of the pulses succeeding a primary avalanche, normalized to the total number of primary events, for different operating conditions, are shown in the right part of fig. 2. Such distributions are characterized by two contributions: the correlated events, representing the effective afterpulses distribution and the uncorrelated background representing the pure thermal noise of the detector.

Afterpulses happening in the first hundreds of nanoseconds, *i.e.* during the operating voltage recovery, are not detected since their amplitude is still under discriminator threshold.

A comparison between dark counting probability and total afterpulsing probability in a  $10 \mu\text{s}$  window, was performed through the subtraction of the uncorrelated background and successive integration of the distributions. In table I are reported the results of such a procedure. As expected a temperature dependence can be observed, however afterpulsing contribution decreases less rapidly compared to the uncorrelated thermal dark count.

## 2. – $5 \times 5$ array

A photomultiplier based on the silicon technology represents the new frontier of the photo-detection. SPADs integrated on the same substrate, with a common readout, could

TABLE I. – *Total afterpulsing probability and the dark count probability, evaluated by integrating the events in a  $10\mu\text{s}$  window, after the subtraction of the uncorrelated background.*

$T$ ( $^{\circ}\text{C}$ )	Excess voltage (%)	Afterpulsing probability	Dark events on $10\mu\text{s}$
15	9.67	$7.69 \times 10^{-4}$	$1.40 \times 10^{-3}$
20	9.67	$8.53 \times 10^{-4}$	$2.75 \times 10^{-3}$
25	9.67	$1.73 \times 10^{-3}$	$9.96 \times 10^{-3}$

satisfy such expectations. The proposed configuration is able to detect and count the impinging photons giving an output pulse directly proportional to the source intensity (like a photomultiplier), that was excluded for the single device operating in Geiger mode. By using Metal-Resistor-Semiconductor structures it is possible to realize devices together with their integrated quenching circuitry; resistive elements are chosen and embedded for each individual micro-cell, providing the effective feedback for stabilization and quenching of the avalanche process.

With this aim, a first prototype of array, with 25 identical devices, in square geometry ( $5 \times 5$ ), was designed and manufactured [8]. The integrated device was designed with a circular  $20\mu\text{m}$ -diameter active area and with centre-to-centre distances ranging from 160 to  $240\mu\text{m}$ . The wiring was realized as in fig. 1.

Differently from the single element, in the array configuration the local gettering region uniformly surrounds the active area of each pixel through an external ring doped by heavy phosphorus diffusion, which also provides the decrease in the dark counting rate. A sampling on dark counting rates on 30 equal arrays of  $5 \times 5$  equal elements has shown a very narrow statistical distribution with an average value of about 400 cps and a dispersion of 50 cps [14].

Limitations to the photon counting arise from the integration of adjacent devices; cross-talk effect as the spurious uncorrelated avalanches triggered in the neighbouring devices and due to the optical and/or electric induction can increase the detector noise.

i) Optical cross-talk: the avalanche multiplication process in a  $p$ - $n$  junction reversely biased over the breakdown value, can lead to the production of secondary photons ([20] and references therein) by radiative emission from the hot carriers. This can lead to the possibility to originate further avalanches in the nearby detectors with a probability which was estimated in  $10^{-5}$  photons per carrier crossing the junction; for near UV and visible photons the attenuation length, in silicon, was of the order of  $80\mu\text{m}$ . Such contribution then represents the fast component of the cross-talk and may be minimized by both, a suitable optical isolation among the diodes (if the pixels are very closed) or by a reduction of the total number of hot carriers crossing the junction.

ii) Electrical cross-talk: electrical induction can occur when carriers, generated during the avalanche process, can overcome the junction, reaching and triggering, the nearby devices and representing the slow component of the cross-talk.

iii) Wiring: a further contribution arises also from the pixels wiring, it may become important when the density of implemented elements is high and the distances between the wiring become smaller.

In order to avoid the optical cross-talk, during the fabrication of arrays of SPAD-STM a delicate process connects “trenches” with metal-coated sidewalls (into the bulk of semiconductor) between pixels, reducing the minimum distance between elements and

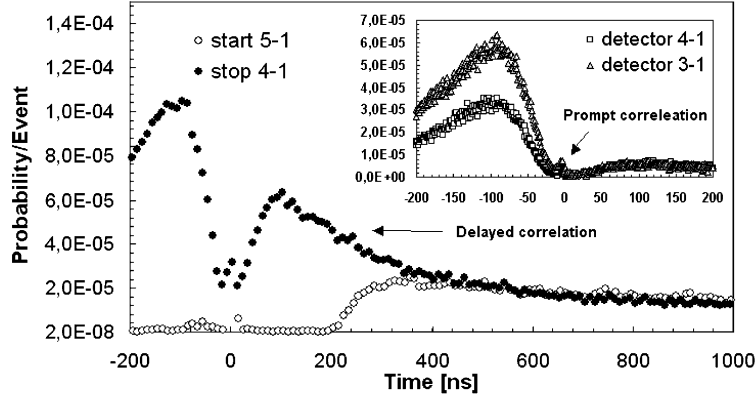


Fig. 3. – Spectra of the pixels 5-1 and 4-1 normalized to the total number of starts.

increasing the dynamic range of the device. This is a delicate process because metal is posed close to the pixel after a difficult previous removing from the active region. Actually, arrays of SPAD-STM optically and electrically isolated by deep thin trench technology were designed and fabricated.

Detailed cross-talk analysis was performed in several steps; primarily the correlation between the array signals was investigated simply by using a digital oscilloscope and the layout of fig. 1.

The possible electric and electromagnetic contribution between the two detectors was studied: choosing a pixel as reference (triggered by a dark event) the induction on both neighbouring and far rows was measured.

As expected from the high pitch values the samples with and without trench show the same behaviour, moreover, the signals comparison shows the presence of a small pulse of opposite polarity with respect to the signal trigger with a timing structure very close to the reference signal but with an amplitude ten times lower. Such contribution was interpreted as a consequence of substrate resistivity which can lead to the propagation of small field fluctuation in the other detectors of the structure.

The next step on the cross-talk investigation was performed by means of the time-correlated measurements between a couple of elements of array. We triggered a data acquisition system, based on Multi-hits TDC, with the dark event on one of the two detectors and we observed the correlated signal on the other. Moreover, in order to get more accurate information on the optical cross-talk component we measured both arrays with and without the optical isolation trenches without finding any significant difference.

The time spectra of the two detectors (the trigger and the correlated one) are reported in fig. 3 after their normalization to the total number of starts and in order to get the probability per event.

As in the previous case, concerning the afterpulsing measurement, the spectrum of the trigger detector (5-1) shows both the contributions of the afterpulses and the uncorrelated dark events with the modulation, in the first hundreds of nanoseconds, of the quenching mechanism and the successive recharging phase.

Similar structures were observed for the correlated stop detector (4-1) where the spectrum can be divided in two temporal regions: before and after the zero time which signs the arrival of trigger signal on the start detector (5-1).

The correlated events, before the zero time, are related to the primary avalanches generated inside the stop detector influencing the start detector. On the contrary, all the events succeeding the zero time are in correlation with the primary avalanches generated in the start detector. In the whole spectrum is also present a flat contribution due to the uncorrelated events.

Assuming a cross-correlation between the two detectors, the ratio between the yields of the two regions is equal to the dark counting rates ratio of the detectors.

From a more careful analysis, the correlation can be classified in: i) a prompt component which disappears in a few ns and centred around the time zero with a probability of the order  $10^{-5}$ , ii) a delayed component which rises and falls in a few  $\mu$ s with a fast growing in few hundreds of ns and with a total strength of the order of  $10^{-3}$ . Such delayed contribution have a trend quite similar to the afterpulsing phenomenon even if its duration seems a little bit faster. Moreover it is important to stress how in this case the spectrum is unaffected by the modulation due to the recharging phase. An increase of the prompt and delayed contributions with increasing excess bias voltage was also observed.

Through further investigation of several groups of pixels with different distances, no substantial differences were found. We conclude that for the  $5 \times 5$  array prototypes the cross-talk phenomenon is under control.

### 3. – SiPM configuration test

A silicon-based photomultiplier SiPM represents one of the major goals of the photonics technology. Today, the common readout of bi-dimensional arrays like SPADs is considered the most promising solution for achievement of this aim [21, 22].

In this section the first results of a  $5 \times 5$  array of SPADs mounted in SiPM configuration will be presented.

SiPM configuration results from the parallel readout of every SPAD element, each one of which is passively quenched by means of a ballast resistor of 100 k $\Omega$ ; output signal is detected on the common load resistor  $R_L$  which connects all the anodes to the ground. In this architecture, the signal is the sum of all the individual cells fired by the photon-initiated avalanche phenomenon. Each single SPAD element operates as a binary device, while their combination makes the device an analogue detector. The output current signal observed to an oscilloscope manifests a multiple structure with several amplitudes: for example, when two photons are simultaneously detected by two (different) pixels a signal with double amplitude was expected; and so on, when  $n$  photons are simultaneously detected manifests a multiple structure with several amplitudes.

To test the whole devices as a function of the number of impinging photons, the array was illuminated by a picosecond laser ( $\lambda = 670$  nm), adjustable in intensity and in repetition rate. The array was biased at 10% of the EBV, cooled at the steady temperature of 20 °C, the output signal was processed by using an amplitude to digital converter (ADC) and the results have been reported in fig. 4. The measured amplitude distribution shows several peaks corresponding to the detection of a single (double, triple, etc.) photoelectron(s). Such results demonstrate, also in this hybrid configuration, the excellent performance of the device in terms of single-photoelectron resolution.

These results were interpreted also by using the output of a Monte Carlo simulation which reconstructs the amplitude signal distribution of arrays taking into account the single detectors response and the cross-talk effects. In particular such code simulates the amplitude distribution of signals from an array illuminated by a laser pulse, starting

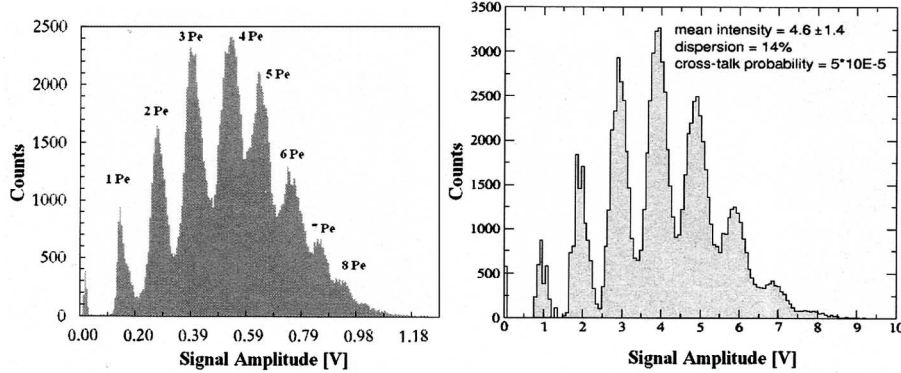


Fig. 4. – Left: amplitude distribution of signals from the  $5 \times 5$  array of SPADs once illuminated by a laser pulse of  $\lambda = 670$  nm. Right: Monte Carlo simulation of signals amplitude distribution of  $5 \times 5$  SPADs array in SiPM configuration once illuminated. See the text for the input parameters.

from the single pixel response in terms of profile, total duration, rise and fall time. The code takes into account also the non-uniformity of the pixels response. The input parameters were: i) the laser intensity and its dispersion, representing the number of fired pixels normally distributed, ii) the percentage of non-uniformity among all the pixels, essentially due to the hybrid configuration, external circuitry, solders, etc., iii) the cross-talk probability, assumed with an infinite interaction range, iv) the dark counting rate.

The values of parameters that better reproduce the experimental distribution are reported in fig. 4; the extracted 14% of non-uniformity parameter was in reasonable agreement with the experimental observation. It appears that an increasing non-uniformity generates an asymmetric distortion of the amplitude distribution and the cross-talk acts on the Gaussian-like background shifting the distribution towards high photoelectron peaks.

#### 4. – Conclusion

The really promising results obtained with Single-Photon Avalanche Diode (SPAD) manufactured by ST-microelectronics in terms of PDE, dark counting rate, timing, afterpulsing probability, demonstrate how SPAD is an ideal candidate among the existing single-photon sensors.

Also the integration possibility, investigated with  $5 \times 5$  arrays manufacture, and the good performance obtained in terms of dark counting rate uniformity and cross-talk contribution seems very promising, especially for the future SiPM realization.

#### REFERENCES

- [1] COVA S. *et al.*, *IEEE J. Quantum Electron.*, QE-19 (1983) 630.
- [2] MCINTYRE R. J., *IEEE Trans. Electron. Dev.*, ED-13 (1966).
- [3] MCINTYRE R. J., *J. Appl. Phys.*, **32** (1961) 983.
- [4] GOETZBERGER A. *et al.*, *J. Appl. Phys.*, **34** (1963) 1591.
- [5] HAITZ R. H., *J. Appl. Phys.*, **35** (1964) 1370.

- [6] HAITZ R. H., *J. Appl. Phys.*, **36** (1965) 3123.
- [7] SCIACCA E. *et al.*, *Mat. Sci. Semicon. Proc.*, **4** (2001) 159.
- [8] SAVELIEV V. *et al.*, *Nucl. Instrum. Methods Phys. Res. A*, **442** (2000) 223.
- [9] BUZHAN P. *et al.*, *Nucl. Instrum. Methods Phys. Res. A*, **504** (2003) 48.
- [10] RIPAMONTI G. *et al.*, *Solid State Electron.*, **28** (1985) 925.
- [11] HEISLMAIR H. *et al.*, *Emis. Data Rev.*, EM 020 ch 15.
- [12] LACAITA A. *et al.*, *Electron. Lett.*, **25** (1989) 13.
- [13] SCIACCA E. *et al.*, *IEEE Trans. Electron. Dev.*, **50** (2003) 4.
- [14] SCIACCA E. *et al.*, *IEEE Photon. Tech. Lett.*, **18** (2006) 15.
- [15] BELLUSO M. *et al.*, *Mem. Soc. Astron. Ital. Suppl.*, **9** (2006) 430.
- [16] TUDISCO S. *et al.*, *Nucl. Phys. B*, **150** (2006) 317.
- [17] TUDISCO S. *et al.*, *Proc. SPIE*, **5864** (2005) 177.
- [18] COVA S. *et al.*, *Appl. Opt.*, **35** (1996) 1956.
- [19] PRIVITERA S., Ph.D dissertation (2006).
- [20] LACAITA A. *et al.*, *IEEE Trans. Electron. Dev.*, **40** (1993) 3.
- [21] CAMPISI A. *et al.*, *Nucl. Instrum. Methods A*, **571** (2007) 350.
- [22] DOLGOSHEIN B., *Nucl. Instrum. Methods A*, **563** (2006) 368.